BRNO UNIVERSITY OF TECHNOLOGY
VYSOKÉ UČENÍ TECHNICKÉ V BRNĚ

FACULTY OF INFORMATION TECHNOLOGY
FAKULTA INFORMAČNÍCH TECHNOLOGIÍ

DEPARTMENT OF COMPUTER GRAPHICS AND MULTIMEDIA
ÚSTAV POČÍTAČOVÉ GRAFIKY A MULTIMÉDIÍ

PLANNING OF OPTIMAL FLIGHT TRAJECTORY
PLÁNOVANÍ OPTIMÁLNÍ TRAJEKTORIE LETU

BACHELOR'S THESIS
BAKALÁŘSKÁ PRÁCE

AUTHOR **MARTIN STUDENÝ**
AUTOR PRÁCE

SUPERVISOR **doc. Ing. PETER CHUDÝ, Ph.D. MBA**
VEDOUCÍ PRÁCE

BRNO 2018

Abstract

This bachelor's thesis deals with the topic of planning of optimal flight trajectory with respect to minimum time intercept of moving target. Differencial equations of motion expanded by the Singular Perturbation Techniques for trajectory optimalization are used for these purposes.

Abstrakt

Tato bakalářská práce řeší problematiku plánování optimální trajektorie letu s ohledem na minimální čas dostihnutí pohybujícího se cíle. Při řešení tohoto problému jsou použity základní diferenciální rovnice pohybu rozšířené o "Singular Perturbation" metodu pro optimalizaci trajektorie letu.

Keywords

Simulation, modeling, optimalization, equations of motion, Singular Perturbation, coordinate systems, trajectory, aircraft intercept, minimum time intercept, aerodynamics

Klíčová slova

Simulace, modelování, optimalizace, rovnice pohybu, Perturbační metoda, souřadnicové systémy, trajektorie, dostihnutí letadla, aerodynamika

Reference

STUDENÝ, Martin. *Planning of Optimal Flight Trajectory.* Brno, 2018. Bachelor's thesis. Brno University of Technology, Faculty of Information Technology. Supervisor doc. Ing. Peter Chudý, Ph.D. MBA

Planning of Optimal Flight Trajectory

Declaration

Hereby I declare that this bachelor's thesis was prepared as an original author's work under the supervision of doc. Ing. Peter Chudý Ph.D. MBA. All the relevant information sources, which were used during preparation of this thesis, are properly cited and included in the list of references.

.....
Martin Studený
July 29, 2019

Acknowledgements

I would like to thank to my supervisor, doc. Ing. Peter Chudý Ph.D. MBA for his guidance, patience and dedicated time.

Contents

List of Figures

List of Tables

List of Acronyms

ECEF	Earth-Centered,Earth-Fixed Frame
NED	North-East-Down frame
ENU	East-North-Up frame
BFF	Body Fixed Frame
WGS-84	World Geodetic System 1984
GPS	Global Positioning System
6DOF	Six degrees of freedom
AoA	Angle of Attack
AoS	Angle of Sideslip
CLME	Conservation of the linear momentum equations
CAME	Conservation of the angular momentum equations
FPE	Flight path equations
KE	Kinematic equations
GE	Gravity equations
3D	Three dimensional
SPT	Singular Perturbation Theory
NASA	National Aeronautics and Space Administration
F-4	McDonnell Douglas F-4
USN	United States Navy
ISA	International Standard Atmosphere

List of Symbols

English

O	origin of coordinate system
x	coordinate x
y	coordinate y
z	coordinate z
h	height, altitude, step
cg	center of gravity
V	velocity
F	force
m	mass
g	gravity acceleration
u	linear velocity
v	linear velocity
w	linear velocity
p	rotation rate
q	rotation rate
r	rotation rate
L	moment
M	moment
N	moment
I_x	moment of inertia
I_y	moment of inertia
I_z	moment of inertia
I_{xz}	product of inertia
c_{D_1}	drag coefficient
c_{L_1}	lift coefficient
c_{m_1}	pitch moment coefficient
q	dynamic pressure
c	mean aerodynamic chord, speed of sound
S	wing surface

Greek

Φ	latitude
λ	longitude
θ	Euler angle
ψ	Euler angle
ϕ	Euler angle
α	Angle of Attack (AoA)
β	Angle of Sideslip (AoS)
δ_E	deflection of the elevators
i_H	deflection of the stabilators

Subscript

e	Earth-Centered frame (ECEF)
n	North-East-Down frame (NED)
b	Body-Fixed frame (BFF)
s	Stability axes
w	Wind axes
A	Aerodynamics
T	Thrust

Chapter 1

Introduction

This thesis is devoted to understanding of differential equations used in aircraft spatial motion. The goal of this application is to study and find an optimal flight path trajetory with respect to minimum time intercept.

Imagine the situation where the we are F-4 pilot of United States Army. Suddenly, the information of strange behavior of Boing 737-800 detected by radar is received. Boing suddenly changed the direction and the communication with it is lost. Action must be taken immediately. So, the task is to get a visual contact with target and wait for further orders. For a problem kind of that, the application that finds the optimal flight path trajectory to get there is implemented.

The organization of this thesis is as follows. The first chapter presents the describtion of aircraft motion in space. Various coordinate systems will be introduced followed by equations describing the aircraft spatial movement. Then, the second chapter deals with a problem of minimum time intercept. So, another equations directly involved in the problem like that are delivered. The implementation details including a problem specifications are discussed in Chapter 4. The evaluation of created trajectories and discussion of possible improvements are introduced in Chapter 5.

Chapter 2

Spatial Aircraft Movement

This chapter deals with the theory of coordinate systems, which is necessary for understanding of aircraft motion. Since aircraft have six degrees of freedom, the description of the position and orientation can be relatively complex. Therefore, number of various frames are usually used. Each of them is using for different situations, what means that it is also necessary to talk about the transformation between them.

The last section of this chapter is dedicated to the aircraft dynamics as an equations of motion expanded by aerodynamic modelling.

2.1 Coordinate Systems

Before derivating of any differential equation describing the aircraft dynamics, it is neccessary to start with definition of ground and body reference frames. It is critical to understand that Newton's second law is valid only by using inertial frame as a reference frame. It means that the reference frame is not accelerating or rotating. Despite the fact that Earth rotate around its own axis, the Earth-based system is assumed to be inertial enough to satisfy the conditions under which Newton's second law is valid. [14]

Even though there are many various systems, this section will describe only the most important ones.

2.1.1 Earth-Centered, Earth-Fixed Frame

As the name implies the Earth-Centered, Earth-Fixed frame (ECEF) (see fig. 2.1) is a three dimensional Cartesian coordinate system attached to the Earth. It causes the system is rotating around its spin axis.

The origin O_e is coincident with a mass center of Earth. Three axis x_e, y_e and z_e are defining the coordinates of the aircraft. The axis x_e intersects the prime meridian with the equator, the axis z_e is directed along the rotation axis towards the North Pole and the y_e is orthogonal to axes x_e and z_e. By using these coordinates, it is simple to define any given point p on the Earth. [4, 12]

2.1.2 Geodetic Coordinate System

Geodetic Coordinate System (see fig. 2.2) is widely used in GPS navigations and it is quite similar to ECEF. The main difference between them is that the ECEF is using the

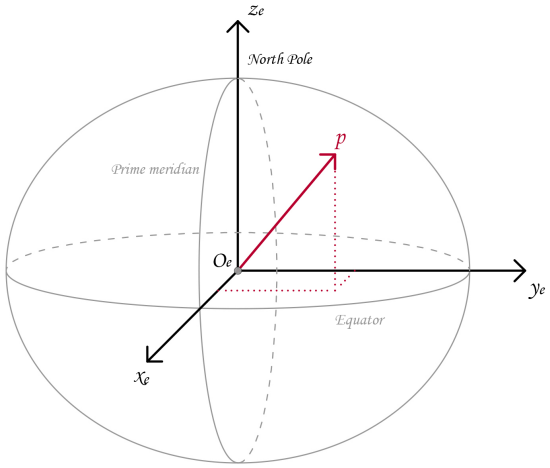

Figure 2.1: Earth-Centered, Earth-Fixed Frame

coordinates for the description of position. On the other hand, geodetic system is using the angles.

Moreover, geodetic system requires of using a reference ellipsoid, such as one defined by World Geodetic System 1984 (WGS-84). The reason for that is that the Earth is not, in fact, perfectly round. Instead, to an excellent approximation the shape of the earth is that of an oblate spheroid. [6]

The two angles Φ and λ determinate the latitude and longitude. It is important to note, that the geodetic latitude and the geocentric latitude are not the same. Geodetic one is defined with reference to local normal. Therefore, it does not cross the origin O_e, as shown in 2.3. The altitude h is also measured along the local normal. It is defined as the distance above reference ellipsoid. [13, 12]

2.1.3 Local Geographic Frames

There are many situations where the simplier coordinate system is preferable to use. In these cases, one of the local geographic frame is used (see fig. 2.2). These types of frames assume that the aircraft flies above a flat ground. For that reason, they are not suitable in scenarios where the aircraft travels far away from its origin. [10, 13]

It is possible to choose between two basic local geographic frames. One of them is East-North-Up (ENU), the second one is North-East-Down (NED). Both are the cartesian coordinate systems with their origin at the point in question. However, ENU is used in situations when objects of interest are above the reference subject. When they are below the reference subject, it is sensible to define down as a positive number, so NED is used. [13]

The origin O_n is arbitrarily fixed to a point on the surface of the Earth. The x_n axis points toward the ellipsoid north. The y_n is perpendicular to the x_n axis and is directed to the ellipsoid east. The right-hand coordinate system is completed with the z_n axis pointing downward along the ellipsoid normal. As shown in figure 2.2, the x_n and y_n axis together define a local horizontal plane tangent to Earth's surface. [4]

In aviation, the origin of NED placed at the center of gravity of the aircraft is commonly demanded. For these needs the extension of NED, referred to as *Vehicle-Carried North-East-Down coordinate system*, is used. [4]

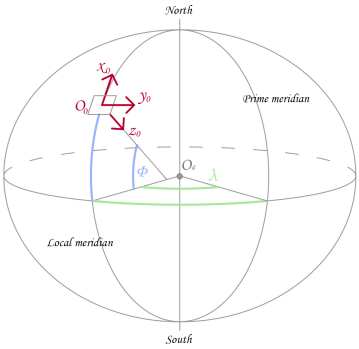

Figure 2.2: NED and geodetic coordinate system

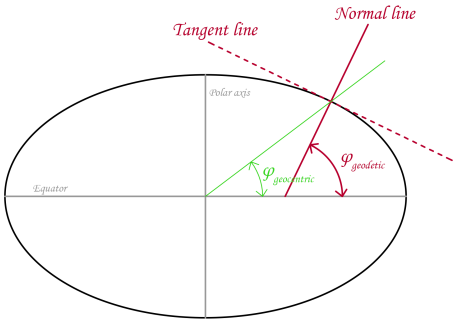

Figure 2.3: Geodetic and geocentric latitude

2.1.4 Body Fixed Frame

As the name suggests, Body Fixed Frame (BFF) is directly fixed to the body of the aircraft. Thus when the aircraft is disturbed from its initial flight conditions the axes move with the airframe and the motion is quantified in terms of variables referred to the moving axes. [7]

The origin is located at the aircraft's center of gravity. The set of axes are indicated with the subscript „b“ and they are defined as follows [12]:

- the x_b axis intersects the nose of the aircraft,
- the y_b axis is directed outward toward the aircraft right wing,
- the z_b axis is directed downwards.

As I already mention earlier, the aircraft has six degrees of freedom (6DOF). It means that there are six ways that the body can move. Not only that it can move along the axes x_b, y_b and z_b, but also, as you can see in fig. 2.4, it is free to rotate in three dimensions: yaw, pitch and roll.

By yawing the rotation around vertical axis between x_b and z_b is meant. Moving between x_b and y_b is called pitching and rotating around longitudinal axis indicates the rolling. [9]

2.1.5 Stability and Wind Axes

The modelling of the aircraft dynamics is based on the use of body fixed frame. However, a different reference frame is needed for modelling the aerodynamics forces and moments acting on aircraft. For this purpose, the Stability and Wind axes are used. [14]

Whereas the Stability and Wind axes (see fig. 2.5) are fixed to the aircraft body, two single rotations of BFF are used for their definition. One for the Stability axes establishment, the second one for the establishment of Wind axes. The detailed description of these rotations are described in chapter 2.2.2.

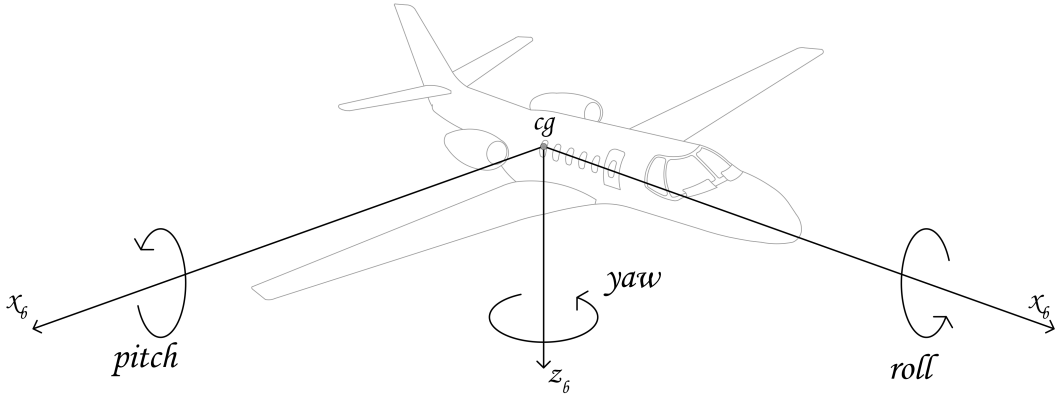

Figure 2.4: Body Fixed Frame

The Stability axes x_s, y_s and w_s are defined with property of the x_s axis being aligned with the direction of the airspeed vector V. As the vertical axis y_s and y_b are the same, the angle between them, α, define the pitch of the aircraft also known as the Angle of Attack (AoA).

Such as the x_s, the wind axis x_w is aligned with flight vector V as well. It is made by the single rotation around the z_s. The angle β of this rotation is known as the Angle of Sideslip (AoS). [1, 14]

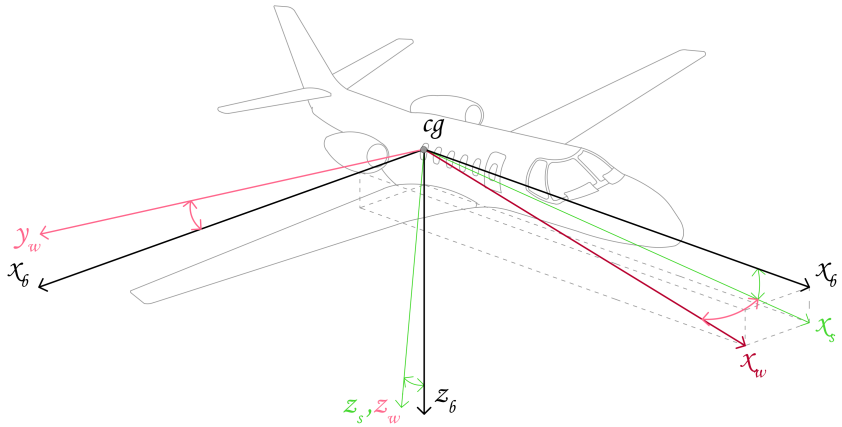

Figure 2.5: Stability and Wind Axes

2.2 Transformations Between Coordinate Systems

As mentioned earlier, the coordinate systems described in section 2.1 are used at various situations. Therefore, it is important to define the way to transfer any given frame into another. The transformation relationships among the coordinate frames are introduced in this section.

2.2.1 North-East-Down to Body-Fixed-Frame

First and foremost, it is necessary to explain usage of the Euler angles. There are many ways how to make the transformation between two coordinate systems. However, the method based on the Euler angles is the most commonly used and all the transformations described in this thesis will be using that method.

General spatial rotation can be separated into three directions. That is exactly what the Euler angles are doing. Let's assume that the origins of the BFF and the NED are all aligned in one same spot. Then, the rotations from NED to BFF could be expressed as a consecutive rotations through three angles, denoted by ψ, θ and ϕ. It must be noted that these rotations are not commutative and they have to be performed in a specific order. With reference to figure 2.6, the three rotations are defined in this order: [1, 12]

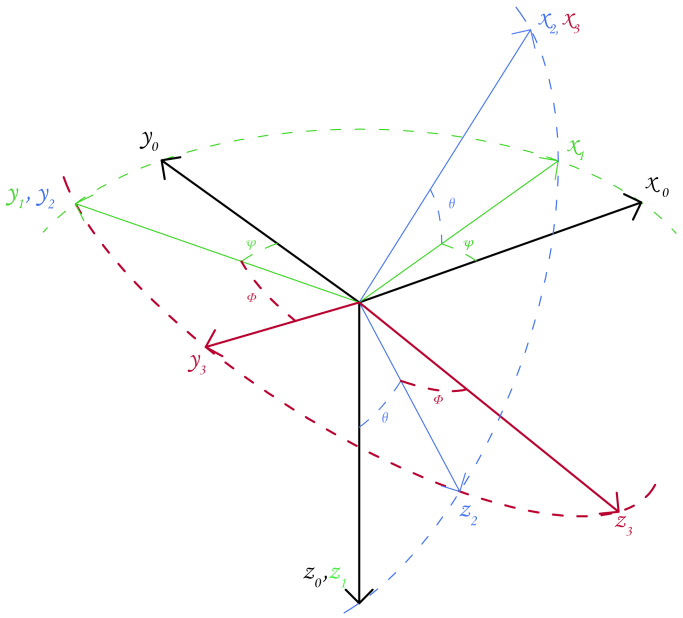

Figure 2.6: Euler angles

1. Rotation around z_0 axis of an angle ψ from the frame x_0, y_0, z_0 to a new frame x_1, y_1, z_1,

$$R_3(\psi) = \begin{bmatrix} \cos\psi & \sin\psi & 0 \\ -\sin\psi & \cos\psi & 0 \\ 0 & 0 & 1 \end{bmatrix} \tag{2.1}$$

2. Rotation around y_1 axis of an angle θ from the frame x_1, y_1, z_1 to a new frame x_2, y_2, z_2,

$$R_2(\theta) = \begin{bmatrix} \cos\theta & 0 & -\sin\theta \\ 0 & 1 & 0 \\ \sin\theta & 0 & \cos\theta \end{bmatrix} \tag{2.2}$$

3. Rotation around x_2 axis of an angle ϕ from the frame x_2, y_2, z_2 to a new frame x_3, y_3, z_3.

$$R_1(\phi) = \begin{bmatrix} 1 & 0 & 0 \\ 0 & \cos\phi & \sin\phi \\ 0 & -\sin\phi & \cos\phi \end{bmatrix} \tag{2.3}$$

The NED to BFF transofrmation matrix T_{NB} is then given by multiplying the rotation matrices of Euler angles.

$$\begin{aligned} T_{NB} &= R_1(\phi)\, R_2(\theta)\, R_3(\psi) \\ &= \begin{bmatrix} \cos\theta\cos\psi & \cos\theta\sin\psi & -\sin\theta \\ \sin\phi\sin\theta\cos\psi - \cos\phi\sin\psi & \sin\phi\sin\theta\sin\psi + \cos\phi\cos\psi & \sin\phi\cos\theta \\ \cos\phi\sin\theta\cos\psi + \sin\phi\sin\psi & \cos\phi\sin\theta\sin\psi - \sin\phi\cos\psi & \cos\phi\cos\theta \end{bmatrix} \end{aligned} \tag{2.4}$$

2.2.2 Body Fixed Frame to Stability and Wind Axes

The rotation from the body fixed system into stability and wind system is done by using the α (AoA) and β (AoS). The rotation matrix (equation 2.5) provide the transforamtion from BFF to Stability axes. Furthermore, the equation 2.6 makes the rotation from Stability axes to Wind axes. [1, 12]

$$T_{BS} = R_{BS}(\alpha) = \begin{bmatrix} \cos\alpha & 0 & -\sin\alpha \\ 0 & 1 & 0 \\ \sin\alpha & 0 & \cos\alpha \end{bmatrix} \tag{2.5}$$

$$T_{SW} = R_{SW}(\beta) = \begin{bmatrix} \cos\beta & -\sin\beta & 0 \\ \sin\beta & \cos\beta & 0 \\ 0 & 0 & 1 \end{bmatrix} \tag{2.6}$$

Then, by appropriately combining of them, the final transformation from BFF to Wind axes, T_{BW}, is made by:

$$T_{BW} = R_{BS}(\alpha)\, R_{SW}(\beta) = \begin{bmatrix} \cos\alpha\cos\beta & -\cos\alpha\sin\beta & -\sin\alpha \\ \sin\beta & \cos\beta & 0 \\ \sin\alpha\cos\beta & -\sin\alpha\sin\beta & \cos\alpha \end{bmatrix} \tag{2.7}$$

2.3 Aircraft Dynamics

The purpose of this section is to provide a detailed understanding of the flight dynamics. Several sets of equations will be derived with respect to an inertial ECEF as well as a BFF. These equations are key to understand the dynamics of aircraft in space.

Then, the more detailed definition of forces and moments acting on aircraft will be introduced.

2.3.1 Equations of Motion

The equations of motion for a flight vehicle are usually written in a body-fixed coordinate system (BFF). Also it is necessary to recall the Newton's second law of motion, which states that the summation of all external forces acting on a body is equal to the time rate of change of the momentum of the body. And that the summation of the external moments acting on the body is equal to the time rate of change of the moment of angular momentum. [15]

The forces and moments acting on the aircraft are gravitational, aerodynamic or caused by an engine thrust. In addition, the aerodynamics forces and moments could be split into lateral and longitudinal component.

Furthermore, The equations are derivered with assumption that the aircraft is assumed to be a rigid body and that its mass is assumed to be constant. This assumption might seem unrealistic considering the fuel consumption. However, it can be sonsidered acceptable over a limited amount of time. [14]

A block diagram showing the integration of equation in this chapter is given in fig 2.7.

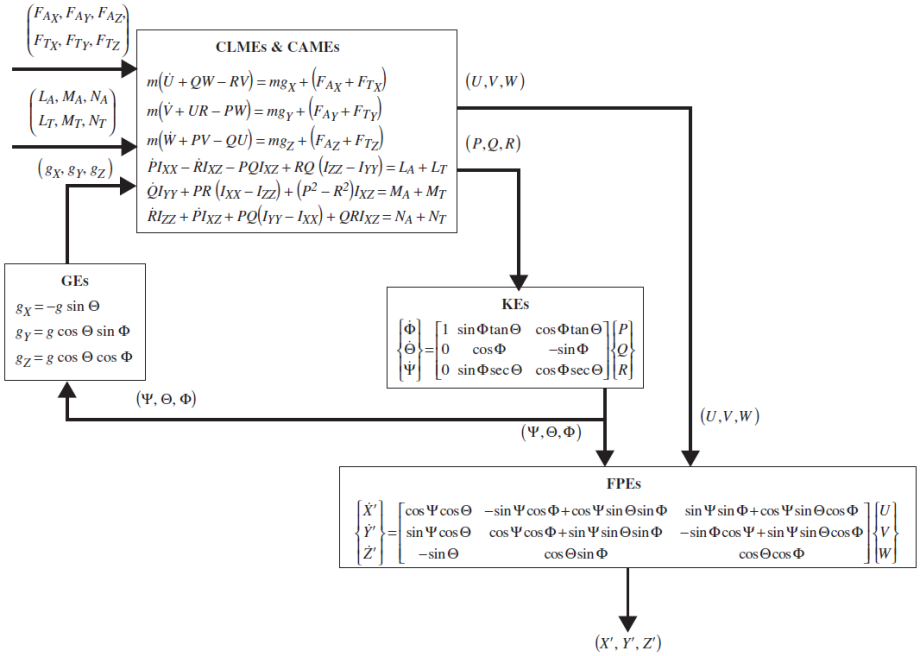

Figure 2.7: Integration of the CLME, CAME, KE, FPE and GE

Linear Momentum Equations

The first set of equations is focused on the forces acting on the aircraft. These equations are based on conservation of linear momentum (CLME) and it's derived by the simplest form of Newton's second law for each differential element of mass in the vehicle, then integrating over the entire vehicle. [5, 14]

$$d\vec{F} = \vec{a}\, dm \tag{2.8}$$

The contributions to its velocity from linear velocities (u, v, w) in each of the coordinate directions as well as the contributions due the rotation rates (p, q, r) about the axes are

taken into account. Resulting in the following set of equations:

$$\begin{aligned} m(\dot{u} + qw - rv) &= mg_x + (\underline{F_{A_x}} + \underline{\underline{F_{T_x}}}) \\ m(\dot{v} + ur - pw) &= mg_z + (\underline{F_{A_y}} + \underline{\underline{F_{T_y}}}) \\ m(\dot{w} + pv - qu) &= mg_z + (\underline{F_{A_z}} + \underline{\underline{F_{T_z}}}) \end{aligned} \tag{2.9}$$

The single underlined forces stand for the aerodynamics forces acting on aircraft during the flight. The double underlined forces stand for the thrust forces acting on the aircraft. They will be introduced later on in this chapter as well as the modeling of gravity components.

By expressing the derived velocities and simplified all the forces into f_x, f_y, f_z, we get these set of equations:

$$\begin{aligned} \dot{u} &= rv - qw + f_x \\ \dot{v} &= pw - ru + f_y \\ \dot{w} &= qu - pv + f_z \end{aligned} \tag{2.10}$$

Angular Momentum Equations

The conservation of angular momentum equations (CAME) are realization of the rotational form of Newton's second law, just like a CLME. However, the moments components (L, M, N), product of inertia (I_{xz}) and moments of inertia (I_x, I_y, I_z) are used instead of forces and velocities. [12, 5]

$$\begin{aligned} \dot{p}\, I_x - \dot{r}\, I_{xz} - pq\, I_{xz} + rq\,(I_z - I_y) &= \underline{L_A} + \underline{\underline{L_T}} \\ \dot{q}\, I_y + pr\,(I_x - I_z + (p^2 - r^2) I_{xz}) &= \underline{M_A} + \underline{\underline{M_T}} \\ \dot{r}\, I_z - \dot{p}\, I_{xz} + pq(I_y - I_x) + qr\, I_{xz} &= \underline{N_A} + \underline{\underline{N_T}} \end{aligned} \tag{2.11}$$

Once again, the single underline moments are the aerodynamic moments, the double underlined moments are the thrust moments. Similiarly to CLME, the $\dot{p}, \dot{q}, \dot{r}$ rotations need to be expressed. [14]

$$\begin{aligned} \dot{p} &= \frac{I_y - I_z}{I_x} qr - \frac{I_{xz}}{I_x}(pq + \dot{r}) + \frac{L}{I_x} \\ \dot{q} &= \frac{I_z - I_x}{I_y} pr - \frac{I_{xz}}{I_y}(p^2 r^2) + \frac{M}{I_y} \\ \dot{r} &= \frac{I_x - I_y}{I_z} pq + \frac{I_{xz}}{I_z}(qr - \dot{p}) + \frac{N}{I_z} \end{aligned} \tag{2.12}$$

Flight Path Equations

The differencial equations (2.3.1 and 2.3.1) describes the motion of the aircraft with respect to the BFF. However, different set of equations is needed for the expression of the trajectory of the aircraft with respect to the ECEF.

Then, the proper equations based on the Euler's angles (described in 2.2) are derived, resulting in the matrix 2.13. The solution of the FPE provides the complete 3D trajectory of the motion of the aircraft. [14]

$$\begin{Bmatrix} \dot{x}_e \\ \dot{y}_e \\ \dot{z}_e \end{Bmatrix} = \begin{bmatrix} \cos\psi\cos\theta & -\sin\psi\cos\phi + \cos\psi\sin\theta\sin\phi & \sin\psi\sin\phi + \cos\psi\sin\theta\cos\phi \\ \sin\psi\cos\theta & \cos\psi\cos\phi + \sin\psi\sin\theta\sin\phi & -\sin\phi\cos\psi + \sin\psi\sin\theta\cos\phi \\ -\sin\theta & \cos\theta\sin\phi & \cos\theta\cos\phi \end{bmatrix} \begin{Bmatrix} u \\ v \\ w \end{Bmatrix} \tag{2.13}$$

Kinematic Equations

The purpose of the Kinematic equations (KE) is to determinte an expression for the Euler angles in terms of rates of change of the components of the aircraft angular velocity p, q, r. [14]

Similarly to FPE, the derivation of the KE will be based on the transformations introduced in chapter 2.2. The solution of the KE provides the numerical values of the Euler angles (ϕ, θ, ψ). The expression for the KE in a matrix format is given by:

$$\begin{Bmatrix} \dot{\phi} \\ \dot{\theta} \\ \dot{\psi} \end{Bmatrix} = \begin{bmatrix} 1 & \sin\phi\tan\theta & \cos\phi\tan\theta \\ 0 & \cos\phi & -\sin\phi \\ 0 & \sin\phi\sec\theta & \cos\phi\sec\theta \end{bmatrix} \begin{Bmatrix} p \\ q \\ r \end{Bmatrix} \tag{2.14}$$

Gravity Equations (GEs)

The last equations needed for understanding of the basics of aircraft dynamics are Gravity equations (GE). The GE are necessary for expressing the components of the gravity vector acting on the aircraft. It may be resolved into components corresponding with axes x_b, y_b and z_b, denoted by g_x, g_y, g_z, respectively. [7, 14]

$$\begin{aligned} g_x &= -g\sin\theta \\ g_y &= g\cos\theta\sin\phi \\ g_z &= g\cos\theta\cos\phi \end{aligned} \tag{2.15}$$

By fitting these variables into CLME, we get these final equations:

$$\begin{aligned} m(\dot{u} + qw - rv) &= \underline{-mg\sin\theta} + (F_{A_x} + F_{T_x}) \\ m(\dot{v} + ur - pw) &= \underline{mg\cos\theta\sin\phi} + (F_{A_y} + F_{T_y}) \\ m(\dot{w} + pv - qu) &= \underline{mg\cos\theta\cos\phi} + (F_{A_z} + F_{T_z}) \end{aligned} \tag{2.16}$$

2.3.2 Aerodynamic Modelling

One of the most difficult task in the modelling of optimal flight path trajectory is identification of the aerodynamic description of the aeroplane for use in the equations of motion.

It is complicated to find a perfect mathematical model to describe the aerodynamic forces and moments acting on the aircraft. Even if it would be possible to devise pretty accurate models, it would be difficult to handle and fit them in the simple form of equations of aircraft motion described in chapter 2.3.1.

As the flow conditions around the airframe are generally complex, the solution to the problem is to seek simplier approximate aerodynamic models which can can be used in the equations of motion and which represent the aerodynamics properties with acceptable accuracy. [7]

In this case, the aerodynamic forces and moments are splitted into two. The longitudinal direction of aerodynamics will be discussed first in the following section. Then, lateral direction will be examine in the section 2.3.2.

Longitudinal Aerodynamic Forces and Moments

Although the aircraft aerodynamics have already been divided into longitudinal and lateral component, another simplification needs to be done. Therefore, there is a further distribution into aerodynamics of wing, body, horizontal tail and vertical tail.

For the purpose of modelling the longitudinal forces and moments, it is necessary to specify the configuration of the horizontal tail. For conventional architactures two longitudinal control surfaces can be used. It is the elevator with deflection δ_E used for maneuvering and the stabilator with deflection i_H used for trimming.

Returning to the linear and angular momentum equations (2.9 and 2.12) it is noticeable that two longitudinal aerodynamics forces (F_{A_x}, F_{A_y}) and one logitudinal moment (F_{A_z}) need to be defined to complete the equations. [14]

The aerodynamic force F_{A_x} is assigned along the x_s (see fig. 2.5). The modelling of the different effects within the coefficient c_{D_1} is expressed as a function of the variables shown in equation below.

$$\begin{aligned} F_{A_x} &= -c_{D_1} qS \\ c_{D_1} &= f(\alpha, \delta_E, i_H) \end{aligned} \tag{2.17}$$

Aerodynamic moment acting around y_s is given by following equation. Coefficient c_{L_1} is similiary to c_{D_1} function of AoA, deflection of elevators and deflection of stabilators.

$$\begin{aligned} F_{A_{Z_1}} &= -c_{L_1} qS \\ c_{L_1} &= f(\alpha, \delta_E, i_H) \end{aligned} \tag{2.18}$$

The last missing piece of the longitudinal aerodynamics is moment acting around y_s.

$$\begin{aligned} M_A &= c_{m_1} qSc \\ c_{m_1} &= f(\alpha, \delta_E, i_H) \end{aligned} \tag{2.19}$$

where

c_{D_1}	is the aircraft dimensionless drag coefficient
c_{L_1}	is the aircraft dimensionless lift coefficient
c_{m_1}	is the aircraft pitching moment coefficient
q	is the dynamic pressure acting on the aircraft
S	is the reference wing surface
c	is the mean aerodynamic chord
α	is the Angle of Attack
δ_E	is the deflection of the elevators
i_H	is the deflection of the stabilizators

Lateral Directional Aerodynamic Forces and Moments

Similarly to the longitudinal aerodynamics, the lateral forces and moments acting on the aircraft need to be explained. The longitudinal aerodynamics was dealing with horizontal tail. On the other hand, the lateral forces and moments acting on the aircraft are affected especially by the vertical tail.

Therefore, the description of the vertical tail has to be introduced. It is assumed that the aircraft features conventional control surfaces, including ailerons (δ_A) for lateral control and ruddler (δ_R) for directional control. [14]

Let's get back to the equations 2.9 and 2.12 again. Notice that in lateral direction the missing variables are F_{A_y}, L_A and N_A. The lateral force around y_s axis is given by:

$$\begin{aligned} F_{A_y} &= c_{y_1} qS \\ c_{y_1} &= f(\beta, \delta_A, \delta_R) \end{aligned} \tag{2.20}$$

The lateral force coefficient c_{y_1} is as the coefficients of rolling moment c_{l_1} and yawing moment c_{n_1} evaluated as a function of AoS, deflaction of the ailerons and deflection of the ruddler.

To complete the 2.9 and 2.12, the modeling of the rolling and yawing moment is evaluated by flollowing equations:

$$\begin{aligned} L_A &= c_{l_1} qSb \\ c_{l_1} &= f(\beta, \delta_A, \delta_R) \end{aligned} \tag{2.21}$$

$$\begin{aligned} N_A &= c_{n_1} qSb \\ c_{n_1} &= f(\beta, \delta_A, \delta_R) \end{aligned} \tag{2.22}$$

2.3.3 Thrust Forces and Moments

The perforamnces of an aircraft depend on its weight, aerodynamic characterics and the installed engine. Since the modelling of the engines's thrust effects assumes the knowladge of engines themselves, only brief and theoretical knowladge will be introduced.

The modelling depends on the number and the loation of the engines on the aircraft. Each of the installed thrust can be considered as vector T_i for $i = 1, ..., N$, where N is the number of engines.

Furthermore, the vector needs to be expressed with respect to the same axes along which the modelling of aerodynamic forces and moments has been provided. For that reason, the angles Θ and Ψ, called toe-up and toe-in angle, respectively, are used. These angles are expressing the deflection from the BFF.

Based on the assumption that these angels are same for all engines, the components of T_i along the x_b, y_b and z_b are given by:

$$\begin{aligned} T_{i_x} &= T_i \cos\Theta \cos\Psi \\ T_{i_y} &= T_i \cos\Theta \sin\Psi \\ T_{i_z} &= T_i \sin\Theta \end{aligned} \tag{2.23}$$

However, in general the thrust of the engines can be expressed as a function of altitude and Mach number. The maximum thrust of the observed F-4 aircraft is stored as a function of Mach number and altitude in Appendix A. [**?**]

Chapter 3

Optimal Flight Path Trajectory

Despite the fact that the equations described in chapter 2.3 are correct at general flight conditions, the another equations and methods needs to be derived to find a solution for a specific optimalization problem.

The goal of this work is to find a solution of the minimum time intercept. The minimalization of intercept time is subject to the following state and control variable contraints:

$$L \leq WG_{max} \tag{3.1}$$

$$L \leq qsC_{L_\alpha}\alpha_{max} \tag{3.2}$$

$$T_{min}(h,V) \leq T \leq T_{max}(h,V) \tag{3.3}$$

$$q \leq q_{max} \quad , \quad M \leq M_{max}(h) \tag{3.4}$$

where G_{max} is the maximum load factor, α_{max} is the stall angle of attack and the T_{min} and T_{max} are the minimum and maximum thrust levels.[TODO-vysvetlit variables]

The equations decribed in NASA report [16] are directly focusing to the the minimum time intercept of a moving target. These equations are based on usage of Singular perturbation method. So, this method is introduced in the following section.

3.1 Singular Perturbation Theory

The Singular Perturbation method is commonly used in chemical kinetics. However, it can be used in many more industries including aviation. The principle lies in the fact, that some of the componens of equations described in chapter 2.3 are acting faster then the others. [17]

Because of the aircraft dynamics which is characterized by the presence of states whose speeds are widely separated, the Singular perturbaton theory (SPT) is well suited to treat systems such as this. [8]

The benefits of using singular perturbation method are that large numerical problem is separated into a series of smaller ones and that the numericaly unstable equations are solved on separate time scales.

Singular perturbation methods are generally trying to write the solution of equations as power series in a small parameter ϵ. The understanding of SPT leads to the problems in which the ϵ multiplies a derivative. The state equations scaled by power of this ϵ are introduced below.

$$\dot{x} = V\cos\gamma\cos\beta \tag{3.5}$$

$$\dot{y} = V\cos\gamma\sin\beta - V_T\cos\gamma_T \tag{3.6}$$

$$\epsilon\dot{E} = \frac{(T-D)V}{W} \tag{3.7}$$

$$\epsilon^2\dot{\beta} = \frac{L\sin\mu}{mV\cos\gamma} \tag{3.8}$$

$$\epsilon^3\dot{h} = V\sin\gamma \tag{3.9}$$

$$\epsilon^4\dot{\gamma} = \frac{L\cos\mu - W\cos\gamma}{mV} \tag{3.10}$$

It must be noted that these equations are derived with respect to target centered coordinate systems. As you can see in the figure ??, the target is denoted by a subscript of T and the angle of sight line to the target in horizontal plane is expressed by λ.

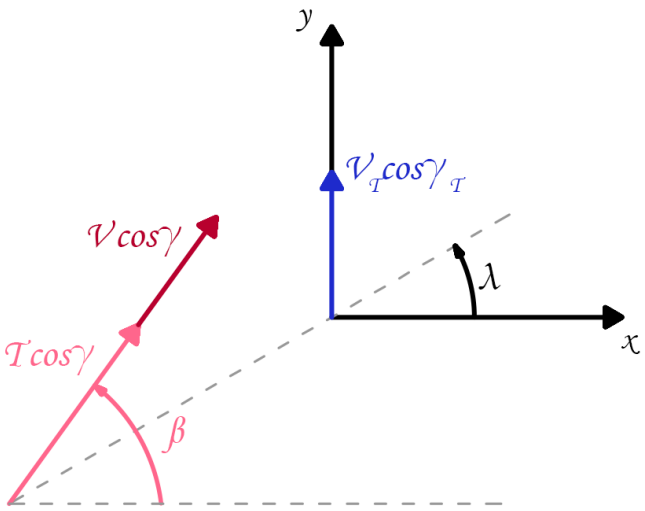

Figure 3.1: Horizontal plane intercept geometry

3.1.1 Outer Solution

As was said before, the solution of equations 3.5 - 3.10 is saparated to the different time scales. The outer solution is then defined by setting the ϵ to zero. Now it is noticeable that by this adjustment, the problem is simplified into two state equations for $\dot{x}$ and $\dot{y}$ only.

$$\dot{x} = V\cos\gamma\cos\beta \tag{3.11}$$

$$\dot{y} = V\cos\gamma\sin\beta - V_T\cos\gamma_T \tag{3.12}$$

$$0 = \frac{(T-D)V}{W} \tag{3.13}$$

$$0 = \frac{L\sin\mu}{mV\cos\gamma} \tag{3.14}$$

$$0 = V\sin\gamma \tag{3.15}$$

$$0 = \frac{L\cos\mu - W\cos\gamma}{mV} \tag{3.16}$$

Since the target velocity is assumed to be constant, the subproblem consists of solving an optimal intercept trajectory only in horizontal plane (see fig. ??). Furthemore, the following conditions must be fulfilled within outer solution:

$$V\sin(\beta-\lambda) = V_T\cos\gamma_T\cos\lambda \tag{3.17}$$

$$T_0 = D_0 \quad \mu_0 = 0 \quad \gamma_0 = 0 \quad L_0 = W \tag{3.18}$$

The control variables for the outer layer solution are h_0 and E_0. These variables are in general equal to the values of height and energy at which the aircraft reach the maximum speed level. The more detailed explanation of value selection of these variables is described in chapterX.

Also, it is important to mention that the energies in the NASA reports are expressed as energy height. That means the unit of these energies are not in joules, but in meters instead. The dependence expression of velocity, height and energy is given by equations 3.19.

$$V = \sqrt{2g(E-h)} \qquad E = \frac{V^2}{2g} + h \tag{3.19}$$

Then, the verification of energy unit is given in following equations:

$$\begin{aligned} V &= \sqrt{2g(E-h)} \\ V^2 &= 2g(E-h) \\ mV^2 + 2mgh &= 2gmE \\ \frac{1}{2}mV^2 + mgh &= mgE \\ E_k + E_p &= mgE \\ [\mathrm{kg}\cdot m^2\cdot s^{-2}] &= [\mathrm{kg}\cdot m^2\cdot s^{-2}] \end{aligned} \tag{3.20}$$

By conditions 3.18 implies that thrust lift is equal to weight in outer solution. In this situation, the outer solution drag variable is given by:

$$D_O = qSC_{D_O} + \frac{KW^2}{qS} \tag{3.21}$$

where dynamic pressure q:

$$q = \frac{\rho(h_o)V_o^2}{2} \tag{3.22}$$

and the V_o is computed by equation 3.19 by using the outer solution energy and height variables. Also, the optimal cruise heading (β_o) needs to be expresed:

$$\beta_o = \sin^{-1}\left(\frac{V_T}{V_o}\cos\gamma_T\cos\lambda\right) + \lambda \tag{3.23}$$

The constates λ_{x_o} and λ_{y_o}, associated with horizontal position dynamics in the outer solution are used in subsequent boundary layers solutions. These take the form:

$$\lambda_{x_o} = \frac{-\cos\beta_o}{V_o - V_T\cos\gamma_T\sin\beta_o} \tag{3.24}$$

$$\lambda_{y_o} = \frac{-\sin\beta_o}{V_o - V_T\cos\gamma_T\sin\beta_o} \tag{3.25}$$

3.1.2 First Boundary Layer

The remaining reduced order problems are called boundary layers and are derived by changing the time scale from t to $\tau = t/\epsilon^i$. The variable i is given by a power of ϵ on the left hand side of equations 3.5 - 3.10.

So, the first boundary layer is generated by setting the time variable in these equations to $\tau = t/\epsilon$ and then letting ϵ approach zero. In this layer, the energy dynamics is addresed with contraints of:

$$\mu_1 = 0, \quad \gamma_1 = 0, \quad L_1 = W \tag{3.26}$$

The controls are thrust T_1, height h_1 and heading β_1. The optimal heading is identical to that for the outer solution. The value of thrust T_1 depends on whether the aircraft is currently climbing or descenting. In case of descent, the energy state constante λ_{E_1} is greater than zero, otherwise gains negative values.

$$\lambda_{E_1} = \frac{WH_o(E, h_1)}{V_1(T_1 - D_o)} \tag{3.27}$$

In the equation of energy state constante, the outer solution Hamiltonian H_o, h_1 and V_1 are missing. The control variable h_1 is obtained by equations 3.28 and 3.29. But since h_1 is independent of target motion, it is precomputed and stored in the series of tables as function of current energy. These tables are shown in appendix A of this work.

$$h_1 = \arg\min\left[\frac{(T_{max} - D_o)V}{V - V_o}\right] \quad \text{, for ascent} \tag{3.28}$$

$$h_1 = \arg\min\left[\frac{-(T_{min} - D_o)V}{V - V_o}\right] \quad \text{, for descent} \tag{3.29}$$

The H_o and V_1 variables are given by following equations:

$$H_o(E, h_1) = \left[\lambda_{x_o}V\cos\beta + \lambda_{y_0}\left(V\sin\beta - V_T\cos\gamma_T\right) + 1\right] \tag{3.30}$$

$$V_1 = \sqrt{2g(E - h_1)} \tag{3.31}$$

3.1.3 Second Boundary Layer

The second boundary layer solution arise when the time transformation $\tau = t/\epsilon^2$ is introduced and if the ϵ is approaching to zero. That results in following contraints:

$$\gamma_2 = 0 \qquad L^2 = L_{22}^2 + W^2 \tag{3.32}$$

The L stands for the total lift and the L_{22} is the horizontal lift component. The control variables in this boundary layer are T_2, h, and L_{22}. Because the angle of heading β is considered to be a faster variable than energy, all turning is assumed to take place near the initial time where $\lambda_{E_1} < 0$. Then the optimal thrust is given only by one equation 3.33.

$$T_2 = T_{max}(h_2, V_2) \tag{3.33}$$

where

$$h_2 = \arg\min\left[\frac{-\rho}{KVH_1(E,h,\beta)}\right] \tag{3.34}$$

and where the $H_1(E,h,\beta)$ is the first boundary Hamiltonian evaluated at current values of E, h, and β. It is expressed by equation 3.35.

$$H_1(E,h,\beta) = \lambda_{x_o} V\cos\beta + \lambda_{y_o}\Big(V\sin\beta - V_T\cos\gamma_T\Big) + \lambda_{E_1}\frac{(T-D_o)V}{W+1} \tag{3.35}$$

The horizontal lift component L_{22} required for the calculations of total lift L and bank angle μ is given by equation 3.36.

$$L_{22} = \sqrt{\frac{-qSWH_1(E,h,\beta)}{VK\lambda_{E_1}}} \tag{3.36}$$

3.2 Proportional Vertical Lift

To avoid the complicate equations of third and fourth boundary layers, the proportional vertical lift is used.

$$\gamma_D = \frac{h_2 - h_1}{\tau_1 V} + \frac{\dot{E}}{V_1}\frac{dh_1}{dE} \tag{3.37}$$

The second term in the above equation is an approxiamtion to the flight path angle for following the first boundary layer climb path. The proportional vertical lift L_{1_p} is computed based on a desired flight path angle rate proportional to $(\gamma_D - \gamma)$:[TODO-upravit]

$$\dot{\gamma_D} = \frac{\gamma_D - \gamma}{\tau_2} = \frac{L_{1_p} - W\cos\gamma}{mV} \tag{3.38}$$

Solving for L_{1_p}:

$$L_{1_p} = mV\frac{\gamma_D - \gamma}{\tau_2} + W\cos\gamma \tag{3.39}$$

The control variables, total lift L and bank angle μ, are then computed as

$$L = \sqrt{L_{1_p}^2 + L_{22}^2} \tag{3.40}$$

$$\mu = \tan^{-1}\left(\frac{L_{22}}{L_{1_p}}\right) \tag{3.41}$$

The values chosen for the F-4 aircraft were $\tau_1 = 15.0$ and $\tau_2 = 6.0$.
The proportional vertical lift is also suitable for the descent trajectory calculations.

Chapter 4

Implementation of Optimal Flight Path Trajectory

This chapter is dedicated to summarize the implementation procedures used for the development of application for optimal flight path trajectory. The first part of this chapter is dedicated to the description of aircraft. Then, used technologies and methods are going to be introduced.

4.1 Aircraft Specification

In this section, the model of McDonnell Douglas F-4 (F-4) used in this work is described. The F-4 is a range supersonic jet interceptor and fight-bomber originally developed for the United States Navy (USN).

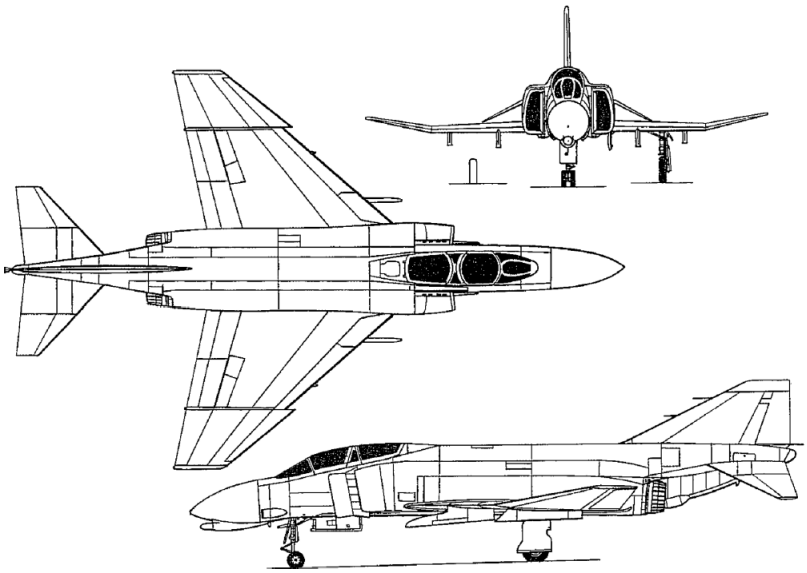

Figure 4.1: 3D View of the McDonnell Douglas F-4 Aircraft

Before doing any real work with equations. it is necessary to specify the parameters of the aircraft of interest. Since the aerodynamic data are depending only on the aircraft velocity, the parameters are stored in table ?? as a function of Mach number.

Table 4.1: Aerodynamic Coefficients for F-4 model as Function of Mach Number

M	C_{D_0}	C_{L_α}	μ
≤ 0.8	0.0130	3.44	0.540
0.9	0.0140	3.58	0.750
1.0	0.0310	4.44	0.800
1.1	0.0388	3.88	0.830
1.2	0.0410	3.44	0.850
1.3	0.0408	3.20	0.875
1.4	0.0390	3.01	0.890
1.5	0.0372	2.84	0.910
1.6	0.0360	2.68	0.920
1.7	0.0354	2.55	0.930
1.8	0.0350	2.44	0.940
1.9	0.0348	2.34	0.945
2.0	0.0346	2.25	0.950

Since small inaccuracies of values of parameters C_{D_0}, C_{L_α}, and μ are negligible to a resulting trajectory, the linear interpolation is used to completeness the missing parameters beween two values of Mach number.

Another variable, that have a singnificant effect on a resulting trajectory is aircraft mass and aerodynamic reference area S. Despite the fact it is unrealistic considering the fuel consumption, the F-4 mass is considered to be a constant with value of 15886 kg. The reference area remains unchanged throughout the fligh and in case of F-4 is equal to 49.293 m^2.

4.2 Implementation

All of the equations desribed in chapter 3.1 are implemented using C programming language. Because the aircraft acquires higher values of velocity at higher altitudes, where the air resistane is lower, the implementation is separated into three parts - climb, cruise, and descent.

At first, the F-4 ascends to the cruise altitude h_o with cruise energy E_o to gain higer value of velocity. However, this causes the problem of choosing the optimal cruise energy E_o for a specific range distances. By that, the intercept can be considered either as long range or short range. As a long range trajectory, the situation where F-4 has enough time to climb to optimal cruise energy (E_0^*) is considered. In our case, the optimal cruise energy $E_0^* = 19100.07$ at the altitude of 9317.89 m.

On the contrary as short range trajectories are considered the situations where F-4 do not have enough time to climb to E_0^* level. Then, the pseudo cruise energy E_o has to be taken into account. The problematics of choosing the pseudo cruise energy level correctly is more detailed introduced in section 4.2.1.

And finally, the last part of the flight trajectory, descent needs to be explained. The implementation problem of descent trajectory lies in finding the right time to start descending to ensure that the interception will occur at the height at which the target is flying.

The second problem is to ensure that the F-4 aircraft will start to descent in the right time. The descent trajectory implementation is desribed in section

4.2.1 Choosing of Cruise Energy

A said before, there is a problem of choosing the right cruise energy level. With reference to NASA documents, several cruise level energies and altitudes are shown in appendix X.

4.2.2 Descent trajectory

4.2.3 Value selection

4.2.4 Target centering projection

4.2.5 Thrust Table Interpolation

4.2.6 Eulerova metoda

4.2.7 ISA model

4.2.8 Intercept detection

4.3 Numerical Methods

Differential equations play a role in the modelling of almost every scientic discipline. Although it is possible to derive solution formulas for some ordinary equations, many of them are so complicated that it is impractical to compute them analytically. In these situation, numerical methods provide powerful solution.

Despite the fact that there are plenty of methods that could be used, the simplest and best known one will be used. [3]

4.3.1 Euler's Method

Euler's method is definitely not the most effective numerical method, but it will be sufficient enough for for the purpose of this study.

First of all, a few notations described in equation 4.1 have to be established. The initial value $Y(t)$ denotes the true solution of the initial value problem with the initial value of Y_0.

The result of Euler's method is an approxiamte solution $y(t)$ at a discrete set of nodes $t_0 < t_2 < ... < t_N \leq t_{end}$

$$\begin{aligned} Y'(t) &= f(t, Y(t)), \\ t_0 \leq \quad t \quad &\leq t_{end}, \\ Y(t_0) &= Y_0 \end{aligned} \tag{4.1}$$

Then, using the initial condition as our starting point, the rest of the solution is generated by these iterative formulas:

$$\begin{aligned} x_{n+1} &= x_n + h \\ y_{n+1} &= y_n + hf(t_n, y_n) \\ n &= 0, 1, ..., N \end{aligned} \tag{4.2}$$

where N is the number of nodes.

The usage example of Euler's method is visualized in fig. 4.2. In order to calculate the value y_{n+1}, the slope of the line tangent to $Y(t)$ at t_n is obtained using the function $f(t_n, y_n)$ and multiplied by the distance of step h. [12, 2]

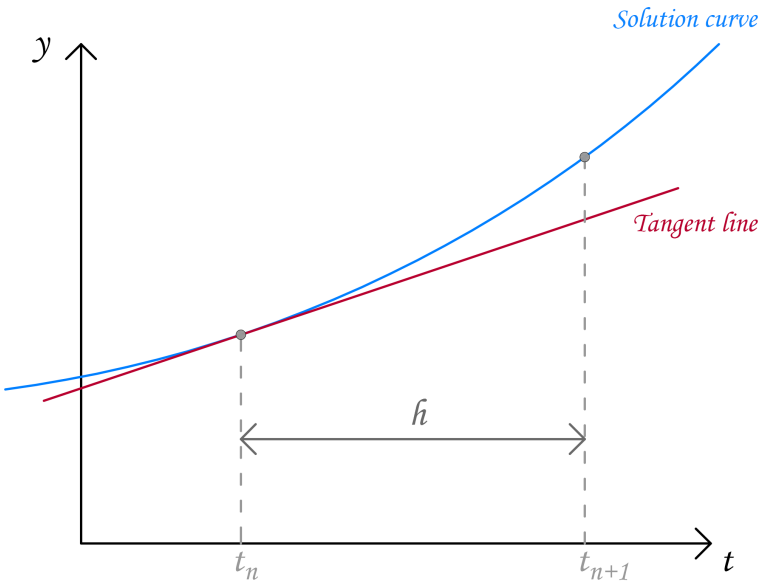

Figure 4.2: Euler's method

As can be seen in the fig. 4.2 the Euler's method is a bit deviated compared to real solution. This noticeable error should be reduced by selecting low value of the step h. Then, the result will be accurate enough, at least for this study. The error will still be much larger then by using more advanced numerical methods.

4.4 Visualization of Results

The resulting solution is stored in the file output.data. Because of the fact that the solution of the minimum time interpcet trajectory is stored in the file `output.data`, some kind of visualization needs to be done to present the results.

4.4.1 GnuPlot

GnuPlot is a portable commnad line driven graphing utility for Linux, OS/2, MS Windows, OSX, VMS, and many other platforms. Gnuplot supports many types of plots in either 2D and 3D, what fits perfectly for our output.

It can draw using lines, points, boxes, contours, vecotr filelds, surfaces and various associated text. It also supprot various specialized plot types. [11]

Also, the gnuplot supports many types of output formats.

Chapter 5

Evaluation

In this chapter the results of the final trajectories are evaluated. For showing of results, three example situations are simualted. First example is focused on a long range trajectory, so the initial distance between F-4 and target aircraft is large enough to climb to optimal cruise energy E_o. In contrast to that, the second case is focused on short range intercept trajectory. At finally, the third example is focused on the situation where F-4 and target have opposite directions at initial condtions.

The initial conditions are visualized in following table tables. The table X shows the initial values for F-4 aircraft, the Y the values of target aircraft.

Table 5.1: Initial F-4 conditions

Case	$x(m)$	$y(m)$	$h(m)$	$\beta(rad)$	V(m/s)
1	0	0	0	1.5708	295.92
2	0	0	3048	0	295.92
3	0	0	3048	0	295.92

Table 5.2: Initial Target conditions

Case	$x(m)$	$y(m)$	$h(m)$	$\beta(rad)$	V(m/s)
1	93023	-53209	3048	0.5	232.56
2	46698	-27000	3048	1.0472	232.56

Case 1

In case number one the distances are large enough to climb to the optimal cruise energy E_0^*. So as expected, the results are as follows:

Case 1

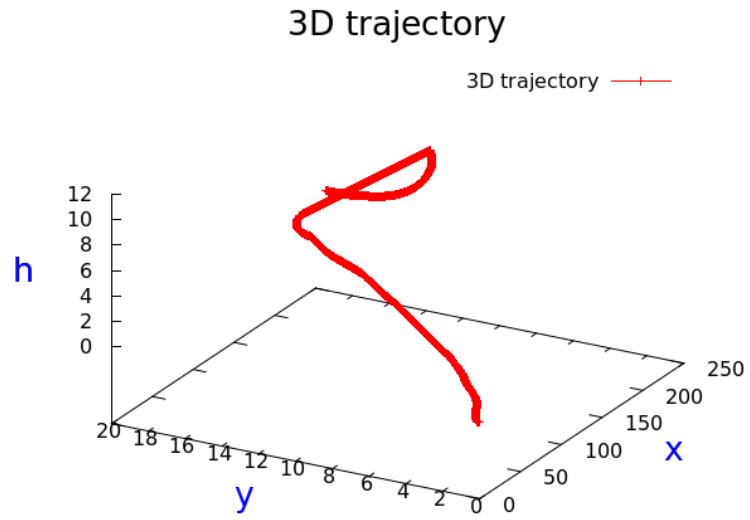

Figure 5.1: 3D visualization

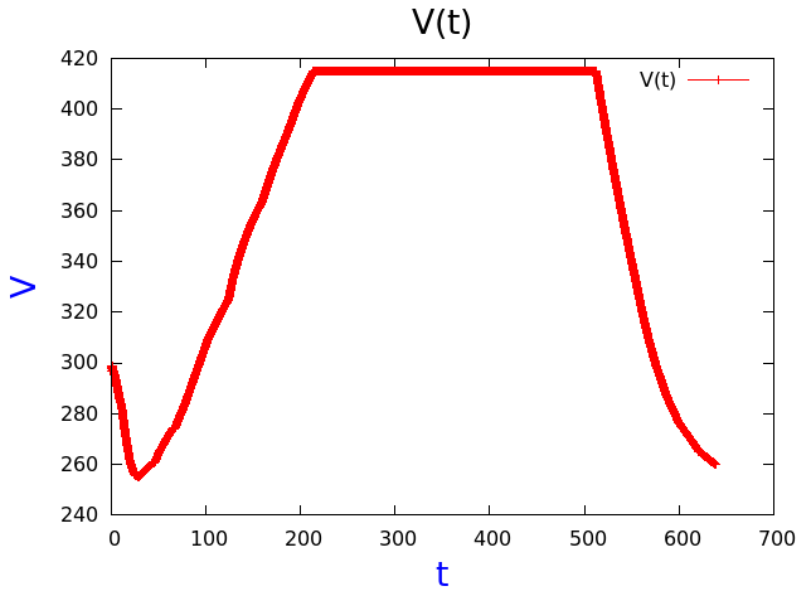

Figure 5.2: V

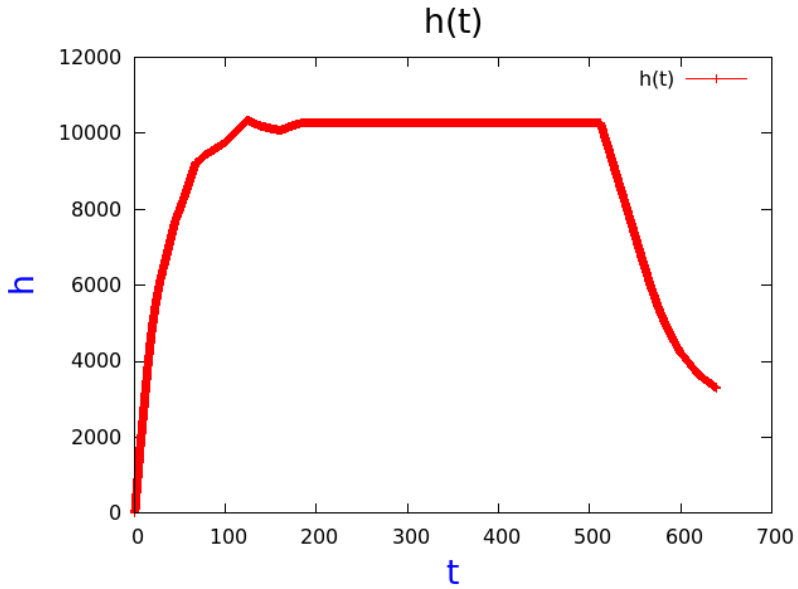

Figure 5.3: h

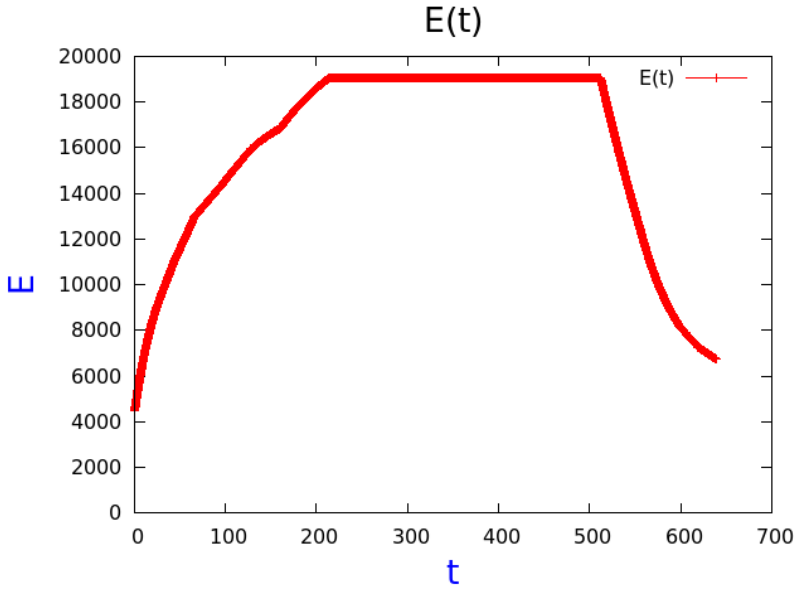

Figure 5.4: E

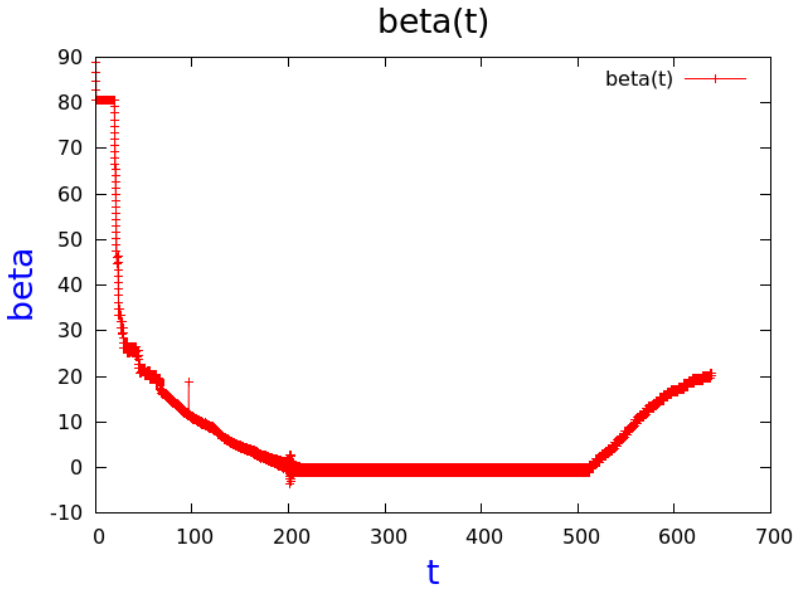

Figure 5.5: Beta

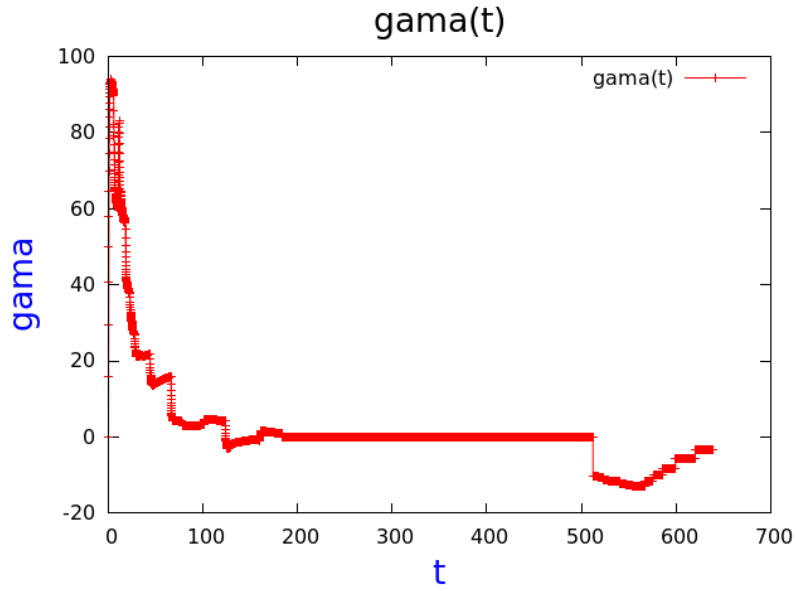

Figure 5.6: gama

Chapter 6

Conclusion

Bibliography

[1] Volume 1. Performance Flight Testing. Chapter 13. Equations of Motion I. Technical Report ADA320205. US Air Force Test Pilot School. 1993.

[2] Anthony J. Calise, D. D. M.: Singular Perturbation Techniques for Real Time Aircraft Trajectory Optimalization and Control. Technical report. NASA - National Aeronautics and Space Administration. 1982.
Retrieved from:
https://ntrs.nasa.gov/archive/nasa/casi.ntrs.nasa.gov/19820023454.pdf

[3] Atkinson, K.: *Numerical Solution of Ordinary Differential Equations*. John Wiley & Sons, Inc.. 1998. ISBN 978-1-118-16452-5.

[4] Butcher, J. C.: *Numerical Methods for Ordinary Differential Equations*. John Wiley & Sons, Inc.. 1996. ISBN 978-1119121503.

[5] Cai, G.; Chen, B. M.; Lee, T. H.: Coordinate Systems and Transformations. In *Unmanned Rotorcraft Systems*. Springer Publishing Company, Incorporated. first edition. 2011. ISBN 0857296345, 9780857296344.

[6] Caughey, D. A.: Introduction to Aircraft Stability and Control. Technical report. Sibley School of Mechanical & Aerospace Engineering. 2011.
Retrieved from: https://courses.cit.cornell.edu/mae5070/Caughey_2011_04.pdf

[7] Collins, G. W.: Coordinate Systems and Coordinate Transformations. In *The Foundations of Celestial Mechanics*. Pachart Publishing House. 2004. ISBN 0881260096, 9780881260090.

[8] Cook, M. V.: *Flight Dynamics Principles: A Linear Systems Approach to Aircraft Stability and Control*. Elsevier Ltd.. second edition. 2007. ISBN 978-0-7506-6927-6.

[9] D.B. Price, D. D. M., A.J. Calise: Piloted Simulation of an Algorithm for Onboard Control of Time-Optimal Intercept. Technical report. NASA - National Aeronautics and Space Administration. 1985.
Retrieved from:
https://ntrs.nasa.gov/archive/nasa/casi.ntrs.nasa.gov/19850020637.pdf

[10] Elmajdub, E. N. F. A.: Modified Six-Degree of Freedom related to Takeoff and Landing stages of Aircraft. In *IOSR Journal of Electrical and Electronics Engineering*. 2017.
Retrieved from: http://www.iosrjournals.org/iosr-jeee/Papers/Vol12%20Issue%205/Version-2/A1205020108.pdf

[11] Hull, D. G.: *Fundamentals of Airplane Flight Mechanics*. Springer-Verlag Berlin Heidelberg. 2007. ISBN 10 3-540-46571-5.

[12] Kelley, T. W. &. C.: *gnuplot 5.0, An Interactive Plotting Program*. Retrieved from: http://www.gnuplot.info/docs_5.0/gnuplot.pdf

[13] Király, A.: Automatic Event identification from Flight Data Records. Technical report. Brno University of Technology, Faculty of Information Technology. 2018.

[14] Koks, D.: Using Rotations to Build Aerospace Coordinate Systems. Technical Report DSTO-TN-0640. Australian Government, Department of Defence. 2008.

[15] Napolitano, M. R.: *Aircraft Dynamics: From Modeling to Simulation*. John Wiley & Sons, Inc.. 2012. ISBN 978-0-470-62667-2.

[16] Nelson, D. R. C.: *Flight Stability and Automatic Control*. McGraw-Hill Book Co. 2011. ISBN 0-07-046273-9.

[17] R. K. Mehra, S. S. J. V. C., R. B. Washburn: A Study of the Application of Singular Perturbation Theory. Technical report. NASA - National Aeronautics and Space Administration. 1979.
Retrieved from:
https://ntrs.nasa.gov/archive/nasa/casi.ntrs.nasa.gov/19790022023.pdf

[18] Roussel, M. R.: Singular perturbation theory. 2004.
Retrieved from: https:
//pdfs.semanticscholar.org/efc3/1aa6a60dfa7086fddf4ad4941b06761dd5d9.pdf

Appendix A

Tables

Maximum thrust Table

Table A.1: Maximum Thrust for F-4 Model as Function of Mach Number and Altitude

$h[m]$ \ $V[M]$	0.4	0.6	0.8	1.0	1.2	1.4	1.6	1.8	2.0
0	12.60	13.70	15.35	16.86	16.06	–	–	–	–
1524	11.21	12.10	13.48	15.26	16.90	16.28	–	–	–
3048	9.74	10.59	11.83	13.52	15.52	17.13	–	–	–
4572	8.32	9.12	10.36	11.92	13.92	16.06	17.21	–	–
6096	7.07	7.70	8.81	10.36	12.14	14.06	15.88	–	–
7620	5.96	6.54	7.47	8.81	10.50	12.50	14.23	15.39	–
9144	4.98	5.47	6.27	7.47	8.94	10.77	12.50	13.83	–
10668	4.05	4.54	5.20	6.18	7.34	8.81	10.40	11.70	12.63
12192	3.25	3.60	4.18	4.98	5.96	7.21	8.59	9.65	10.45
13716	2.54	2.89	3.38	3.96	4.76	5.74	6.81	7.70	8.36
15240	1.96	2.18	2.49	3.02	3.69	4.45	5.29	5.92	6.41
16764	1.42	1.65	1.87	2.27	2.85	3.43	4.09	4.54	4.85
18288	0.98	1.11	1.33	1.65	2.05	2.54	3.02	3.38	3.60
19812	0.58	0.71	0.85	1.07	1.33	1.69	2.05	2.31	2.40
21336	0.31	0.40	0.49	0.62	0.76	0.98	1.29	1.38	1.42

Descent Tables

Table A.2: Descent variables, cruise energy = 19100.07

Cruise energy = 19049.99			
$Energy(m)$	$H(m)$	$Time(s)$	$Range(m)$
3586.91	0.00	357.6738	210690.6
4499.47	677.40	270.8616	208237.4
5412.00	1331.60	198.3982	205738.5
6324.54	1976.64	143.5021	203069.4
7237.08	2604.15	108.2608	200349.5
8149.62	3212.69	87.5223	197458.7
9062.16	3814.46	74.0457	194302.4
9974.69	4390.52	63.7786	190987.3
10887.23	4957.39	55.3226	187502.6
11799.77	5506.95	48.1671	183662.9
12712.30	6030.09	41.5890	179272.1
13624.85	6553.26	35.1294	174160.9
14537.38	7055.07	28.8112	168122.7
15449.92	7531.21	22.6819	160315.6
16362.46	8006.49	16.7482	149984.7
17275.00	8463.37	10.9957	132477.7
18187.54	8896.07	5.4142	95683.5
19100.07	9317.89	0.0000	0.0

Ascent Tables

Table A.3: Ascent variables, cruise energy = 19049.99

Cruise energy = 19049.99			
$Energy(m)$	$H(m)$	$Time(s)$	$Range(m)$
279.45	0.00	628.5549	210690.6
1383.60	0.00	608.0056	208237.4
2487.75	0.00	595.0452	205738.5
3591.90	30.48	584.0422	203069.4
4696.05	822.96	573.5481	200349.5
5800.20	1615.44	562.8831	197458.7
6904.35	2407.92	551.7278	194302.4
8008.50	3596.64	539.8125	190987.3
9112.65	4846.32	527.1221	187502.6
10216.80	5974.08	513.2688	183662.9
11320.95	7071.36	497.5857	179272.1
12425.10	8168.64	479.4856	174160.9
13529.25	9265.92	458.2539	168122.7
14633.39	10027.92	431.6506	160315.6
15737.55	11125.20	397.0964	149984.7
16841.70	10271.76	343.9612	132477.7
17945.85	10668.00	244.0769	95683.5
19049.99	10636.09	0.0000	0.0

Table A.4: Ascent variables, cruise energy = 15737.55

Cruise energy = 15737.55			
$Energy(m)$	$H(m)$	$Time(s)$	$Range(m)$
279.45	0.00	275.9463	78177.2
1383.60	0.00	255.3971	75724.0
2487.75	0.00	242.4366	73225.1
3591.90	30.48	231.4336	70556.0
4696.05	822.96	220.9393	67836.1
5800.20	1615.44	210.2742	64945.3
6904.35	2407.92	199.1189	61789.0
8008.50	3566.16	187.1362	58435.7
9112.65	4663.44	173.9817	54709.5
10216.80	5791.20	159.2435	50510.3
11320.95	6888.48	142.5676	45719.5
12425.10	7985.76	123.3140	40147.4
13529.25	8717.28	99.3018	32953.4
14633.39	9784.08	68.3067	23472.8
15737.55	8370.48	0.0000	0.0
16841.70	0.00	0.0000	0.0
17945.85	0.00	0.0000	0.0
19049.99	0.00	0.0000	0.0

Table A.5: Ascent variables, cruise energy = 13529.25

Cruise energy = 13529.25			
$Energy(m)$	$H(m)$	$Time(s)$	$Range(m)$
279.45	0.00	237.1549	67539.1
1383.60	0.00	216.6056	65085.9
2487.75	0.00	203.6451	62586.9
3591.90	30.48	192.6421	59917.9
4696.05	822.96	182.1478	57198.0
5800.20	1615.44	171.4827	54307.2
6904.35	2407.92	160.3274	51150.8
8008.50	3230.88	147.3731	47332.3
9112.65	4358.64	131.9121	42741.9
10216.80	5486.40	114.7642	37635.2
11320.95	6096.00	92.6095	30741.9
12425.10	7193.28	62.4630	21150.7
13529.25	7034.38	0.0000	0.0
14633.39	0.00	0.0000	0.0
15737.55	0.00	0.0000	0.0
16841.70	0.00	0.0000	0.0
17945.85	0.00	0.0000	0.0
19049.99	0.00	0.0000	0.0

Table A.6: Ascent variables, cruise energy = 11320.25

Cruise energy = 11320.25			
$Energy(m)$	$H(m)$	$Time(s)$	$Range(m)$
279.45	0.00	194.4020	54474.5
1383.60	0.00	173.8526	52021.2
2487.75	0.00	160.8922	49522.3
3591.90	30.48	149.8892	46853.3
4696.05	822.96	139.3948	44133.4
5800.20	1615.44	128.7297	41242.6
6904.35	2407.92	117.5744	38086.2
8008.50	3139.44	104.2652	34120.5
9112.65	3870.96	84.9084	28070.4
10216.80	4541.52	51.5031	17163.0
11320.95	5626.88	0.0000	0.0
12425.10	0.00	0.0000	0.0
13529.25	0.00	0.0000	0.0
14633.39	0.00	0.0000	0.0
15737.55	0.00	0.0000	0.0
16841.70	0.00	0.0000	0.0
17945.85	0.00	0.0000	0.0
19049.99	0.00	0.0000	0.0

Table A.7: Ascent variables, cruise energy = 9112.65

Cruise energy = 9112.65			
$Energy(m)$	$H(m)$	$Time(s)$	$Range(m)$
279.45	0.00	107.9332	25825.6
1383.60	0.00	87.3839	23372.3
2487.75	0.00	74.4234	20873.4
3591.90	30.48	63.4204	18204.4
4696.05	822.96	52.9260	15484.5
5800.20	1615.44	42.2609	12593.7
6904.35	2407.92	31.1056	9437.3
8008.50	3139.44	17.7964	5471.5
9112.65	4065.64	0.0000	0.0
10216.80	0.00	0.0000	0.0
11320.95	0.00	0.0000	0.0
12425.10	0.00	0.0000	0.0
13529.25	0.00	0.0000	0.0
14633.39	0.00	0.0000	0.0
15737.55	0.00	0.0000	0.0
16841.70	0.00	0.0000	0.0
17945.85	0.00	0.0000	0.0
19049.99	0.00	0.0000	0.0

Table A.8: Ascent variables, cruise energy = 6904.35

Cruise energy = 6904.35			
$Energy(m)$	$H(m)$	$Time(s)$	$Range(m)$
279.45	0.00	76.8073	16350.4
1383.60	0.00	56.2579	13897.2
2487.75	0.00	43.2975	11398.3
3591.90	30.48	32.2945	8729.2
4696.05	822.96	21.8001	6009.3
5800.20	1615.44	11.1350	3118.5
6904.35	2477.75	0.0000	0.0
8008.50	0.00	0.0000	0.0
9112.65	0.00	0.0000	0.0
10216.80	0.00	0.0000	0.0
11320.95	0.00	0.0000	0.0
12425.10	0.00	0.0000	0.0
13529.25	0.00	0.0000	0.0
14633.39	0.00	0.0000	0.0
15737.55	0.00	0.0000	0.0
16841.70	0.00	0.0000	0.0
17945.85	0.00	0.0000	0.0
19049.99	0.00	0.0000	0.0

Table A.9: Ascent variables, cruise energy = 4696.05

Cruise energy = 4696.05			
$Energy(m)$	$H(m)$	$Time(s)$	$Range(m)$
279.45	0.00	55.0058	10342.0
1383.60	0.00	34.4565	7888.8
2487.75	0.00	21.4960	5389.9
3591.90	30.48	10.4930	2720.8
4696.05	820.36	0.0000	0.0
5800.20	0.00	0.0000	0.0
6904.35	0.00	0.0000	0.0
8008.50	0.00	0.0000	0.0
9112.65	0.00	0.0000	0.0
10216.80	0.00	0.0000	0.0
11320.95	0.00	0.0000	0.0
12425.10	0.00	0.0000	0.0
13529.25	0.00	0.0000	0.0
14633.39	0.00	0.0000	0.0
15737.55	0.00	0.0000	0.0
16841.70	0.00	0.0000	0.0
17945.85	0.00	0.0000	0.0
19049.99	0.00	0.0000	0.0

Appendix B

Content of the included CD

- `/xstude23-BP.pdf` - electronic version of the thesis
- `/doc.zip` - compressed source files of the thesis
- `/src/` - directory containing the sources files of the implemented application
- `/example/`- directory containing the example trajectory results